Communication

Electron Paramagnetic Resonance Detection of Intermediates in the Enzymatic Cycle of an Extradiol Dioxygenase

William A. Gunderson, Anna I. Zatsman, Joseph P. Emerson, Erik R. Farquhar, Lawrence Que Jr., John D. Lipscomb, and Michael P. Hendrich

J. Am. Chem. Soc., **2008**, 130 (44), 14465-14467 • DOI: 10.1021/ja8052255 • Publication Date (Web): 08 October 2008

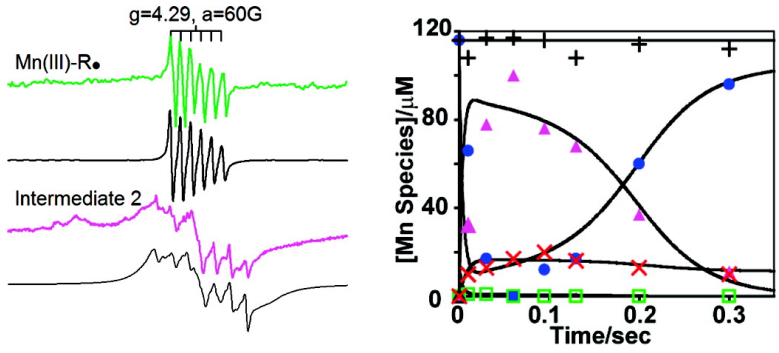

More About This Article

Additional resources and features associated with this article are available within the HTML version:

- Supporting Information
- Access to high resolution figures
- Links to articles and content related to this article
- Copyright permission to reproduce figures and/or text from this article

View the Full Text HTML

J|A|C|S
COMMUNICATIONS

Published on Web 10/08/2008

Electron Paramagnetic Resonance Detection of Intermediates in the Enzymatic Cycle of an Extradiol Dioxygenase

William A. Gunderson,[†] Anna I. Zatsman,[†] Joseph P. Emerson,[‡] Erik R. Farquhar,[‡] Lawrence Que, Jr.,[‡] John D. Lipscomb,[‡] and Michael P. Hendrich*,[†]

Department of Chemistry, Carnegie Mellon University, Pittsburgh, Pennsylvania 15213, and Department of Chemistry and Department of Biochemistry, Molecular Biology and Biophysics, University of Minnesota, Minneapolis, Minnesota 55455

Received July 7, 2008; E-mail: hendrich@andrew.cmu.edu

Extradiol catecholic dioxygenases catalyze the cleavage of the aromatic ring of the substrate with incorporation of both oxygen atoms from O_2.[1] This reaction is a key step in the ability of Nature to reclaim large quantities of carbon sequestered in aromatic compounds. The active sites of these enzymes contain either Mn or Fe, coordinated by a 2-His-1-carboxylate facial triad, which is a common motif of nonheme Fe(II)-containing enzymes that activate dioxygen.[2] Homoprotocatechuate 2,3-dioxygenase from either *Brevibacterium fuscum* or *Arthrobacter globiformis* catalyzes the ring opening of homoprotocatechuate (HPCA) and contains Fe(II) (FeHPCD) or Mn(II) (MnMndD), respectively, as the native metals. Structures of FeHPCD from crystals that had been incubated with the substrate analogue 4-nitrocatechol and then exposed to low concentrations of O_2 identified three intermediate complexes in the catalytic cycle: semiquinone substrate radical-Fe superoxo (**E-SQ**), Fe-alkylperoxo (**E-AP**), and the Fe-semialdehyde ring-opened product (**EP**).[3] Bond length analysis suggests that the iron remains ferrous in each species. A mechanistic proposal developed from these intermediates and earlier studies suggests that electron transfer from the substrate to O_2, via the metal to form the **E-SQ** intermediate, results in simultaneous activation of both substrate and oxygen. Recent work has shown that FeHPCD and MnMndD can each be prepared with the nonphysiological metal in the active site (MnHPCD and FeMndD) and that all four forms have approximately the same catalytic parameters.[4] The fact that FeHPCD and MnHPCD also have superimposable structures suggests that the bound metals retain their inherent ~0.7 V difference in redox potential, leading to the proposal that the metal does not undergo a redox state change in the reaction cycle.

Here we explore this question through direct electron paramagnetic resonance (EPR) detection and quantitative analysis of the metal oxidation states of MnHPCD as it turns over the natural substrate, HPCA. MnHPCD was chosen for study because it is available in a pure state, it is EPR active, and its full length form is structurally characterized. Four distinct Mn species are observed, two of which are short-lived intermediates. Our advances in EPR simulation software[5,6] allow characterization of the electronic environment of all Mn species and the determination of concentrations of all species during turnover. Based on this analysis, a low-concentration intermediate appearing immediately after O_2 addition is found to contain Mn(III) coupled to a radical. Thus, it is possible that the rapid electron transfer to form the reactive **E-SQ** intermediate is not a concerted process, thereby revealing a new aspect of oxygen activation chemistry by this enzyme class.

EPR spectra and simulations of MnHPCD in buffer (50 mM MOPS, pH 7.8) are shown in Figure 1. The substrate-free enzyme

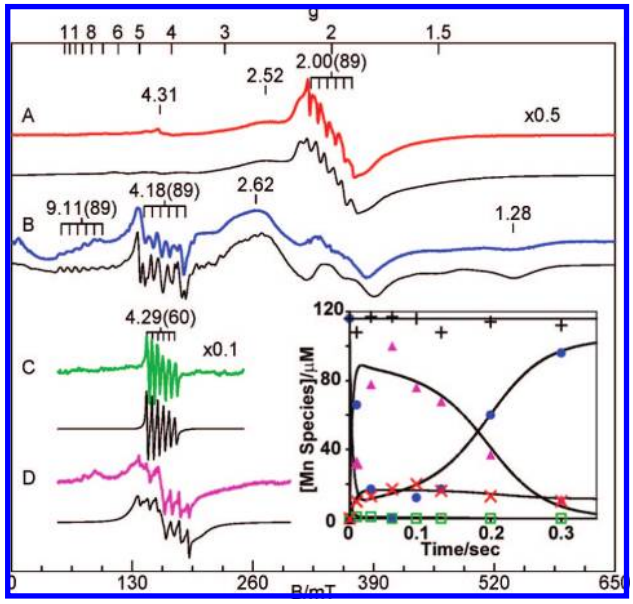

Figure 1. EPR spectra (colored lines) and simulations (black lines) of (A) **E**, (B) **ES**, (C) **I1**, and (D) **I2**. *g*-values are marked with corresponding hyperfine values in Gauss in parentheses. Spectral parameters: microwaves, 9.65 GHz, 0.2 mW; temperature, 11 K (except spectrum C, see text). Simulation parameters all for $S = {}^5/_2$, $I = {}^5/_2$: (A) $g = 2$, $D = 0.055$ cm^{-1}, $E/D = 0.18$, $a = 89$ G; (B) $g = 2$, $D = 0.090$ cm^{-1}, $E/D = 0.18$, $a = 89$ G; (C) $g = 1.995$, $D = 2.5$ cm^{-1}, $E/D = 0.33$, $\mathbf{a} = (63, 75, 43)$ G; (D) $g = 2$, $D = 0.24$ cm^{-1}, $E/D = 0.26$, $a = 89$ G. Inset: All intensities are shown for equimolar species, with additional magnification as indicated. Concentration of Mn species vs time for RFQ samples with $[O_2]/[E_T] = 2.9$: **E** (×), **ES** (●), **I1** (□), **I2** (▲), total Mn (+). The fit is generated numerically for the set of kinetic parameters given in the Supporting Information.

(**E**, Figure 1A) shows a six-line hyperfine pattern centered at $g = 2.00$, with splitting of $a = 89$ G, and a broad feature at $g = 2.52$. The hyperfine constant is indicative of a Mn(II) species, and the simulation of this spectrum (spectrum A) is calculated for a single protein-bound Mn(II) species using the parameters given in the Figure 1 caption. The quantitative simulation determines the species concentration, and this concentration was found to be in agreement with the Mn concentration determined from metal analysis. For all samples of this work, a free Mn(II) species was either absent or insignificant in amount. The weak signal at $g = 4.3$ is an Fe impurity that accounts for less than 2% of the protein concentration.

An excess of substrate HPCA (27 equiv in deaerated buffer) was added to samples of MnHPCD deaerated with Ar. The EPR signal of the substrate-free enzyme vanishes and is replaced by signals which span a much broader field range (Figure 1B). Again, the simulation for a single protein-bound Mn(II) species agrees with

[†] Carnegie Mellon University.
[‡] University of Minnesota.

10.1021/ja8052255 CCC: $40.75

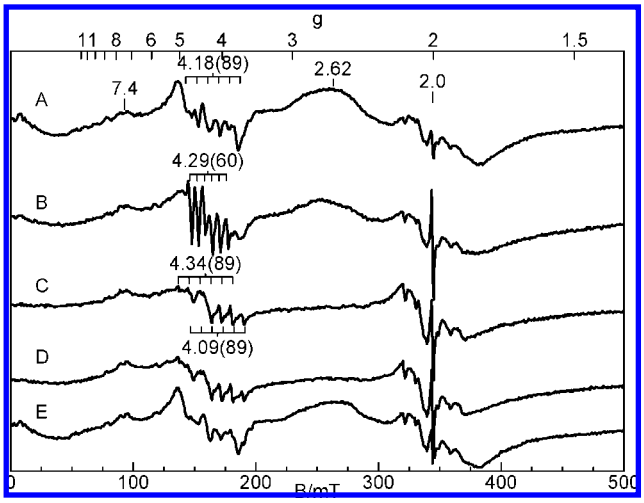

Figure 2. EPR spectra of RFQ samples at (A) 0, (B) 15, (C) 34, (D) 100, and (E) 300 ms. The intensity of each spectrum is corrected for the packing factor of the sample. The spectral parameters are the same as in Figure 1. RFQ conditions prior to mixing: [MnHPCD], 0.45 mM; [HPCA], 12 mM; [O_2], 1.3 mM (saturated); $T = 21$ °C; buffer, 50 mM MOPS, pH 7.8.

the experimental spectrum, and the Mn concentration determined from the simulation is in quantitative agreement with measurement from metal analysis. Thus, all Mn in this sample originates from a single species in which substrate is bound to Mn(II) in the active site (**ES**). Two six-line hyperfine patterns are observed in the spectrum at $g = 9.11$ and 4.18, both with a splitting of $a = 89$ G. The axial splitting parameter for **E** ($D = 0.055$ cm^{-1}) is typical of Mn(II) centers with multiple coordinated water molecules in a distorted octahedral geometry to the Mn.[7] The large increase in this value for **ES** ($D = 0.090$ cm^{-1}) indicates significant changes in the Mn(II) ligand-field and/or ligand covalency due to the binding of the bidentate catecholate and the loss of two water molecules. For both complexes, the sign of D is not determined.

Samples of **ES** were prepared anaerobically as above for use in rapid freeze−quench (RFQ) experiments, where **ES** was mixed with O_2-saturated buffer, quenched into isopentane at −130 °C after varied millisecond times, and packed into EPR tubes. Figure 2 shows EPR spectra at $T = 11$ K of a representative series of reaction time points from 0 to 300 ms. The signal at $g = 7.4$ is from an Fe(III) impurity that does not change in time. We use this signal to correct signal intensities for the variation (at most 20%) in sample packing after RFQ. The spectrum at 0 ms (Figure 2A) is a control sample obtained by quenching substrate-bound enzyme without mixing with O_2-saturated buffer. This spectrum is essentially the same as that of **ES** of Figure 1A.

At 15 ms (Figure 2B), the **ES** signals have 60% of the intensity of the 0 ms sample, indicating that this fraction of the Mn sites has not yet reacted with O_2; 40% of the Mn has reacted and is distributed among three different species. The first of these species, referred to as Intermediate 1 (**I1**), accounts for about 5% of the Mn and has a new six-line hyperfine pattern centered at $g = 4.29$ with $a = 60$ G. In multiple other preparations of the 15 ms sample, the amount of this species was in the range of 2−5%. A second new species, Intermediate 2 (**I2**) is also observed in this region but is not well resolved until later time points. **I2** has a larger a-value and accounts for about 30% of the Mn. Approximately 5% of the Mn is associated with a signal similar to that of **E**. A sharp radical signal at $g = 2.005$ is also observed but has a spin concentration (determined under nonsaturating conditions) of 0.5% of [Mn] and will not be considered further.

At 34 ms (Figure 2C), the **ES** signals have almost vanished, and a small amount of **I1** remains. **I2** is now dominant and accounts for 75% of the Mn; thus, the hyperfine pattern of **I2** is revealed. It consists of two overlapping six-line hyperfine patterns at $g = 4.09$ and 4.34, both with $a = 89$ G. Simulations indicate (see below) that the two hyperfine patterns originate from the same spin doublet. At 100 ms (Figure 2D), **I2** has decreased and **ES** begins to increase. At 300 ms (Figure 2E), the intensity of the **ES** signal has returned to nearly that of the 0 ms sample. The return of the **ES** complex is consistent with the limiting O_2 ([O_2]/[E_T] = 2.9) and excess HPCA ([HPCA]/[E_T] = 27) present in the sample.

We have shown above that assignments for the specific signals from **E** and **ES** are known, and that the concentration of each species can be determined directly from the EPR spectra. We will now consider possible assignments for the signals from the two new intermediates. Variable-temperature studies of the RFQ samples show that the signal of **I1** has maximal intensity at 11 K and vanishes at 2 K, indicating that it originates from an excited spin doublet. The temperature dependence of the signal gives a zero-field splitting of $D = 2.5(5)$ cm^{-1} ($S = {}^5/_2$). All other signals present in the samples display Curie law behavior (intensity $\sim 1/T$). The unique temperature dependence of **I1** allows subtraction of all other Mn signals in the EPR spectrum. This difference spectrum and a corresponding simulation of the signal are shown in Figure 1C for the 15 ms time point. The simulation indicates that **I1** originates from an $S = {}^5/_2$ Mn center. Thus, while the spin state suggests a Mn(II) species for **I1**, the large zero-field splitting and small hyperfine splitting ($a_{iso} = 60$ G) are not compatible with Mn(II). Furthermore, the linewidths of the individual hyperfine lines are dependent on the nuclear m_I spin state. This m_I-dependent broadening can be simulated with a 30% anisotropy in the values of the a-tensor.

To our knowledge, all known Mn(II) protein species display EPR signals with D-values less than 0.5 cm^{-1} and isotropic a-tensors with a_{iso}-values that are within 10% of 89 G. The above results indicate that **I1** is not an isolated Mn(II) species and must be from a Mn ion interacting with one or more radical spins. An $S = {}^5/_2$ state could possibly arise from a Mn(II) ion coupled with two radicals: a superoxide radical and a cation radical on the HPCA substrate. A similar description has been invoked for the O_2-bound intermediate of FeHPCD with 4-nitrocatechol, **E-SQ**.[3] However, the a-value of **I1** rules out this active-site configuration as follows. The hyperfine value for a Mn(II) site is related to the threee-spin effective (observed) hyperfine value by either $a_{eff} = (31/35)a_{Mn}$ (Mn(II)-biradical triplet) or $a_{eff} = a_{Mn}$ (Mn(II)-biradical singlet).[8] For both cases, the predicted hyperfine values ($a_{eff} \approx 78$ or 89 G) are too large to be compatible with that observed for **I1** (60 G), and so we must consider other Mn oxidation states. An $S = {}^5/_2$ state could also originate from a Mn(IV) ion and two radicals; however, we also rule this out, since it would require an anion radical for the substrate. Alternatively, an $S = {}^5/_2$ state could originate from a Mn(III) ion that is ferromagnetically spin-coupled to a single radical species. For this configuration, the observed a-value is $a_{eff} = (4/5)a_{Mn}$ and corresponds to $a_{Mn} = 75$ G for **I1**. This value is in the range of the isotropic a-values for known Mn(III) centers in other proteins (64−81 G[6,9]). Furthermore, the anisotropy in the a-tensor for **I1** is comparable to the anisotropy of these proteins (20−30%), and the D-value for **I1** is in the range of values known for Mn(III) centers.[10] Thus, we conclude that **I1** is a Mn(III) ion spin-coupled to a radical center. Two possible Mn(III)-radical moieties envisioned for the active site of HPCD are Mn(III)-superoxide or Mn-peroxo-HPCA radical. At present, we cannot rule out either of these assignments. The ferromagnetic spin state favors assignment to the Mn-superoxide species, since a parallel spin configuration facilitates delocalization of the unpaired superoxide electron into the empty Mn(III) orbital. We know of no precedent for such a Mn species in proteins or synthetic complexes. The reaction of O_2,[11] superoxides,[12]

or peroxides[13] with mononuclear Mn(II) or Mn(III) complexes produces peroxoMn(III) centers, while the reaction of O_2 with Mn(II)-tetraphenylporphyrin produces a peroxoMn(IV) center.[14] A ferromagnetic configuration has been observed for a Cu(II) complex bound to a superoxide radical.[15] Alternatively, the observation of a nitrocatechol radical in the crystal structure of **E-SQ**[3] suggests an assignment of **I1** to a Mn(III)-peroxo-(HPCA radical) species. However, we are also unaware of any metal-aromatic radical centers in coordination complexes or proteins that show a ferromagnetic configuration.

Next, we consider the species associated with **I2**. Its signal at 100 ms and a simulation are shown in Figure 1D. The signal of **I2** has a hyperfine splitting (89 G) and temperature dependence that are typical of Mn(II) species. This signal is clearly not associated with **ES**; the hyperfine patterns are different, and the $g = 2.62$ feature of **ES** is absent. The simulation of **I2** indicates a Mn(II) $S = {}^5/_2$ species with relatively large axial and rhombic distortions for a Mn(II) center.[16] The crystal structures of FeHPCD with 4-nitrocatechol[3] suggest two species that could possibly give rise to an EPR spectrum like that of **I2**, namely, **E-AP** or **EP**. Samples of MnHPCD were prepared with a large excess of HPCA (400 equiv) and then bubbled with O_2 in an effort to generate the product complex. The EPR spectrum of this sample is different from those of both **I2** and **E**, indicating that a new coordination environment of the Mn center has been generated. However, since the product undergoes isomerization after it is formed, this new state may be more relevant to the isomerized product. Nevertheless, the large axial distortion ($D = 0.24$ cm^{-1}) of **I2** is rare for Mn(II) species and is indicative of significant change in the ligand field or ligand covalency at the Mn(II) center.[7a] Such changes in the geometry or covalency may be more compatible with that expected for a Mn(II)-alkylperoxo species.

The simulations of the spectra allow an independent determination of the concentrations of the four species (**ES**, **I1**, **I2**, and **E**) at each time point. These concentrations and the total [Mn] are plotted in the inset of Figure 1. Within experimental uncertainty, the total Mn is conserved at all time points; thus, no significant amounts of Mn go undetected by EPR during turnover. Based on EPR observations, a minimal scheme of the reaction mechanism involving these species (showing their tentative structures) and substrate (S) and product (P) is shown below.

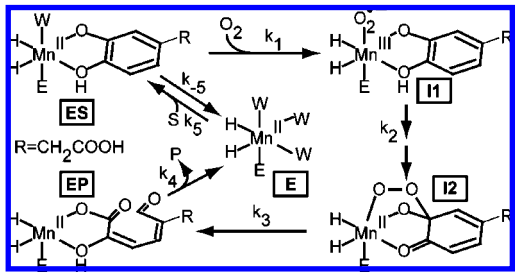

The theoretical curves shown in Figure 1 are generated numerically by choosing a set of kinetic values that fit the data (see Supporting Information). While this set of rate constants is not unique, a good fit to the data is obtained, and the same set of constants gives a good fit to a second set of RFQ experiments conducted with a factor of 4 lower O_2 concentration (Figure S1 in the Supporting Information). Although **I1** accounts for at most 5% of the Mn in our RFQ measurements, the theoretical curves show that this is the expected amount for the kinetic scenario shown above. Other, more complex scenarios involving, for example, branched pathways at **I1** are possible but cannot be evaluated in the absence of concentration-dependent kinetic measurements. However, all fits require that the decay of **I2** (k_3) is the rate-limiting step in the overall reaction mechanism. A tentative assignment of **I2** to a Mn(II)-alkylperoxo species would then implicate the O−O bond cleavage as the overall slow step in the mechanism.

In summary, two intermediates of the reaction of MnHPCD with HPCA have been observed. The most rapidly formed of these species (**I1**) is a Mn(III)-radical species, implicating a redox transformation of the metal during the reaction cycle. Previous studies based on the crystal structures of intermediates in the FeHPCD reaction and steady-state kinetics of both the MnHPCD and FeHPCD suggested that the reactive form is a Mn(II) state with both substrate and O_2 radicals bound. If the new Mn(III) state we observe here occurs as part of a linear series, then it may be that electron transfer from the metal to O_2 occurs more rapidly than that from substrate to the metal during the binding reaction. This may be related to a conversion of the planar aromatic substrate to the nonplanar semiquinone radical for net electron transfer to occur. The resulting diradical pair may then react rapidly to form the alkylperoxo intermediate observed in the crystal structures, and discussed here as **I2**. The rates of the redox steps prior to irreversible and rate-limiting O−O bond cleavage are presumed to be dependent on the metal potential. However, slow O_2 reduction should be complemented by fast substrate oxidation and vice versa, such that the steady-state kinetic parameters may remain metal independent, as previously observed.

Acknowledgment. Financial support for this work is from NIH: GM77387 (M.P.H.), GM24689 (J.D.L.), and GM33162 (L.Q.).

Supporting Information Available: Experimental details for sample preparation, RFQ reactions, low O_2 RFQ data, EPR methods, kinetic analysis, and controls. This material is available free of charge via the Internet at pubs.acs.org.

References

(1) (a) Vaillancourt, F. H.; Bolin, J. T.; Eltis, L. D. *Crit. Rev. Biochem. Mol. Biol.* **2006**, *41*, 241–267. (b) Kovaleva, E. G.; Lipscomb, J. D. *Nat. Chem. Biol.* **2008**, *4*, 186–193. (c) Kovaleva, E. G.; Neibergall, M. B.; Chakrabarty, S.; Lipscomb, J. D. *Acc. Chem. Res.* **2007**, *40*, 475–483.
(2) Vetting, M. W.; Wackett, L. P.; Que, L., Jr.; Lipscomb, J. D.; Ohlendorf, D. H. *J. Bacteriol.* **2004**, *186*, 1945–1958.
(3) Kovaleva, E. G.; Lipscomb, J. D. *Science* **2007**, *316*, 453–457.
(4) Emerson, J. P.; Kovaleva, E. G.; Farquhar, E. R.; Lipscomb, J. D.; Que, L., Jr. *Proc. Natl. Acad. Sci. U.S.A.* **2008**, *105*, 7347–7352.
(5) Golombek, A. P.; Hendrich, M. P. *J. Magn. Reson.* **2003**, *165*, 33–48.
(6) Pierce, B. S.; Hendrich, M. P. *J. Am. Chem. Soc.* **2005**, *127*, 3613–3623.
(7) (a) Smoukov, S. K.; Telser, J.; Bernat, B. A.; Rife, C. L.; Armstrong, R. N.; Hoffman, B. M. *J. Am. Chem. Soc.* **2002**, *124*, 2318–2326. (b) Un, S.; Dorlet, P.; Voyard, G.; Tabares, L. C.; Cortez, N. *J. Am. Chem. Soc.* **2001**, *123*, 10123–10124.
(8) See Supporting Information for additional details of spin interactions.
(9) Zheng, M.; Khangulov, S. V.; Dismukes, G. C.; Barynin, V. V. *Inorg. Chem.* **1994**, *33*, 382–387.
(10) (a) Krzystek, J.; Telser, J.; Hoffman, B. M.; Brunel, L.-C.; Licoccia, S. *J. Am. Chem. Soc.* **2001**, *123*, 7890–7897. (b) Campbell, K. A.; Force, D. A.; Nixon, P. J.; Dole, F.; Diner, B. A.; Britt, R. D. *J. Am. Chem. Soc.* **2000**, *122*, 3754–3761.
(11) Shook, R. L.; Gunderson, W. A.; Greaves, J.; Ziller, J. W.; Hendrich, M. P.; Borovik, A. S. *J. Am. Chem. Soc.* **2008**, *130*, 8888–8889.
(12) (a) Groni, S.; Blain, G.; Guillot, R.; Policar, C.; Anxolabehere-Mallart, E. *Inorg. Chem.* **2007**, *46*, 1951–1953. (b) VanAtta, R. B.; Strouse, C. E.; Hanson, L. K.; Valentine, J. S. *J. Am. Chem. Soc.* **1987**, *109*, 1425–1434.
(13) (a) Seo, M. S.; Kim, J. Y.; Annaraj, J.; Kim, Y.; Lee, Y.-M.; Kim, S.-J.; Kim, J.; Nam, W. *Angew. Chem., Int. Ed.* **2007**, *46*, 377–380. (b) Kitajima, N.; Komatsuzaki, H.; Hikichi, S.; Osawa, M.; Moro-oka, Y. *J. Am. Chem. Soc.* **1994**, *116*, 11596–11597.
(14) Hoffman, B. M.; Weschler, C. J.; Basolo, F. *J. Am. Chem. Soc.* **1976**, *98*, 5473–5482.
(15) Lanci, M. P.; Smirnov, V. V.; Cramer, C. J.; Gauchenova, E. V.; Sundermeyer, J.; Roth, J. P. *J. Am. Chem. Soc.* **2007**, *129*, 14697–14709.
(16) The simulation includes an Fe(III) impurity at $g = 4.3$ which is 2% of the Mn concentration.

JA8052255